Accessory Cholera Enterotoxin, Ace, from Vibrio cholerae: Structure, Unfolding, and Virstatin Binding

ARTICLE *in* BIOCHEMISTRY · MARCH 2011

Impact Factor: 3.02 · DOI: 10.1021/bi101673x · Source: PubMed

6 AUTHORS, INCLUDING:

Tanaya Chatterjee
Bose Institute
19 PUBLICATIONS **284** CITATIONS
SEE PROFILE

Debadrita Mukherjee
Bose Institute
4 PUBLICATIONS **13** CITATIONS
SEE PROFILE

Sucharita Dey
Bose Institute
10 PUBLICATIONS **222** CITATIONS
SEE PROFILE

Mirajul Kazi
National Institute of Cholera and Enteric Dis…
28 PUBLICATIONS **300** CITATIONS
SEE PROFILE

BIOCHEMISTRY
including biophysical chemistry & molecular biology

ARTICLE

pubs.acs.org/biochemistry

Accessory Cholera Enterotoxin, Ace, from *Vibrio cholerae*: Structure, Unfolding, and Virstatin Binding

Tanaya Chatterjee,[*,†] Debadrita Mukherjee,[†] Sucharita Dey,[‡] Aritrika Pal,[†] Kazi Mirajul Hoque,[§,∥] and Pinak Chakrabarti[*,†,‡]

[†]Department of Biochemistry and [‡]Bioinformatics Centre, Bose Institute, P-1/12 CIT Scheme VIIM, Kolkata 700054, India

[§]Division of Molecular Pathophysiology, National Institute of Cholera and Enteric Diseases, P-33, CIT Road, Scheme-XM, Beliaghata, Kolkata 700 010, India

[∥]Department of Medicine, Gastroenterology Division, Johns Hopkins University, Baltimore, Maryland 21205, United States

Supporting Information

ABSTRACT: *Vibrio cholerae* accessory cholera enterotoxin (Ace) is the third toxin, along with cholera toxin (CT) and zonula occludens toxin (Zot), that causes the endemic disease cholera. Structural characterization of Ace has been restricted because of the limited production of this toxic protein by *V. cholerae*. We have cloned, overexpressed, and purified Ace from *V. cholerae* strain O395 in *Escherichia coli* to homogeneity and determined its biological activity. The unfolding of the purified protein was investigated using circular dichroism and intrinsic tryptophan fluorescence. Because Ace is predominantly a hydrophobic protein, the degree of exposure of hydrophobic regions was identified from the spectral changes of the environment-sensitive fluorescent probe 4,4′-dianilino-1,1′-binaphthyl-5,5′-disulfonic acid (bis-ANS) that quenches the fluorescence of tryptophan residues of Ace in a concentration-dependent manner. Results showed that bis-ANS binds one monomeric unit of Ace with a 1:1 stoichiometry and a K' of 0.72 μM. Ace exists as a dimer, with higher oligomeric forms appearing upon glutaraldehyde cross-linking. This study also reports the binding of virstatin, a small molecule that inhibits virulence regulation in *V. cholerae*, to Ace. The binding constant ($K = 9 \times 10^4$ M^{-1}) and the standard free energy change ($\Delta G^\circ = -12$ kcal mol^{-1}) of Ace−virstatin interaction have been evaluated by the fluorescence quenching method. The binding does not affect the oligomeric status of Ace. A cell viability assay of the antibacterial activity of Ace has been performed using various microbial strains. A homology model of Ace, consistent with the experimental results, has been constructed.

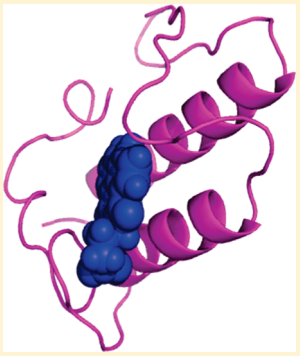

Vibrio cholerae is a Gram-negative comma-shaped bacterium that causes the diarrheal disease cholera that results from the interaction of cholera toxin (CT) with intestinal epithelial cells.[1] CT is an adenosine diphosphate-ribosylating toxin, which elevates the level of cyclic adenosine monophosphate (cAMP) in intestinal epithelial cells.[2] The gene encoding Ace is located immediately upstream of the genes encoding CT and Zot, and these three comprise the "virulence cassette" of *V. cholerae*.[3−5]

Ace (Swiss-Prot entry C3M620-1) is an integral membrane protein, which consists of 96 amino acids (11.3 kDa) and has no disulfide bonds. Previous studies showed that Ace has the activity of a classic enterotoxin in an in vivo model (rabbit ileal loops) and in an in vitro model (rabbit Ussing chamber).[5,6] It has been suggested that after infection by *V. cholerae*, Ace may contribute to intestinal secretion and diarrhea before the stimulation of the slow acting CT. Ace stimulates Ca^{2+}-dependent Cl^-/HCO_3^- symporters, thereby creating a potential difference across the membrane, which involves both an influx of extracellular Ca^{2+} across the apical membrane of the cells and intracellular Ca^{2+} stores. Though the mechanism of action of Ace is reported in the literature,[6] a comprehensive and systematic characterization of this toxin, especially from the structural point of view, is still elusive. This is mainly because of the low level of production of the toxin by *V. cholerae*. Moreover, there was difficulty in the purification of Ace, as *ace* clones in *Escherichia coli* are unstable, resulting in cell lysis.[7] This paper describes cloning, overexpression, and purification of toxin Ace from a specialized *E. coli* strain, which has allowed us to conduct comprehensive studies to elucidate structural and functional properties of this toxin.

The far-UV CD spectrum of a protein is a diagnostic probe of secondary structural features that comprise the native conformation.[8,9] By using a combination of fluorescence and circular dichroism (CD) spectroscopy, we have observed that the thermodynamic unfolding of Ace by guanidinium hydrochloride (GdnHCl) follows a two-state transition. 4,4′-Dianilino-1,1′-binaphthyl-5,5′-disulfonic acid (bis-ANS) is an environment-sensitive fluorescent dye whose fluorescence quantum yield increases upon binding to hydrophobic sites of proteins.[10,11] bis-ANS is found to bind to Ace with high affinity. Fluorescence resonance energy transfer (FRET) provides further evidence of the hydrophobic ligand-binding site of Ace. The protein shows

Received: October 18, 2010
Revised: February 28, 2011
Published: March 02, 2011

antibacterial activity against *E. coli*, *Proteus mirabilis*, *Staphylococcus aureus*, and *Pseudomonas aeruginosa*. Finally, the ability of the recombinant Ace to stimulate Cl^- secretion across intestinal epithelial cells has been investigated.

Small molecules have proven to be valuable tools for studying a wide range of biological processes and interaction with various proteins.[12,13] Protein−small molecule interaction is important for understanding the molecular mechanisms of drug action and inhibition of virulent activities. It is challenging, however, to identify such small molecules, which can inhibit virulence activities of pathogenic bacteria. Virstatin {4-[*N*-(1,8-naphthalimide)]-*n*-butyric acid} (Figure S1 of the Supporting Information) is just such a small molecule that attenuates toxin expression in *V. cholerae* by preventing the dimerization of ToxT, which directly activates the virulence genes cholera toxin (*ctxAB*) and the toxin coregulated pilus (*tcp*).[14] By targeting the pathogenic mechanism of *V. cholerae*, it is capable of preventing the colonization of bacteria in mice, even though it fails to kill bacteria in culture.[12] Because of the potentially profound importance of virstatin, we chose to study its effect on the structure of Ace, which is a component of the virulence cassette of *V. cholerae*. In this work, we studied the interaction of Ace with virstatin using various biophysical methods involving fluorescence quenching and far-UV CD. On the basis of fluorescence quenching measurements, the binding constant for the Ace−virstatin complex, as well as the standard free energy of the association, has been estimated. Far-UV CD was used to determine the changes in protein secondary structure upon binding to virstatin. Thermal unfolding of native Ace, and Ace treated with virstatin, has also been studied. Glutaraldehyde cross-linking was also employed to determine the oligomeric status of Ace in the presence of virstatin. A homology model of Ace has been built, and the putative binding site of virstatin is predicted from docking studies.

EXPERIMENTAL PROCEDURES

Materials. *V. cholerae* classical strain O395 was a gift from R. Nandi (National Institute of Cholera and Enteric Diseases). Bacterial strains *P. aeruginosa* MTCC 424, *Pr. mirabilis* MTCC 425, and *S. aureus* MTCC 3160 were obtained from MTCC Chandigarh, and *E. coli* K12 was obtained from S. Roy. Acrylamide, IPTG, and PMSF were purchased from Sigma Chemicals (St. Louis, MO). Taq DNA polymerase, restriction enzymes *Bam*HI and *Sal*I, and dNTPs were purchased from Fermentas. Guanidinium hydrochloride (GdnHCl) was purchased from Calbiochem. T4 DNA ligase was obtained from New England Biolabs, and Ni-NTA Superflow Agarose was from Qiagen. Virstatin was purchased from Merck. All other chemicals, obtained from Merck, were analytical grade.

Cloning, Expression, and Purification of Ace. Genomic DNA isolated from *V. cholerae* O395 was used as template for amplification of the *ace* gene by polymerase chain reaction (PCR), using the primers 5′GTAGGCGGATCCATGCTTAT GATGGACCCC3′ and 5′TCTACGGTCGACGCGCCGTGA TGAATAAAG3′. The purified restriction enzyme-digested PCR product was ligated into the *Bam*HI- and *Sal*I-digested pQE30 plasmid, which was used to transform competent *E. coli* XL1B cells. The fact that the plasmid contains the correct sequence of the *ace* gene was confirmed by DNA sequencing (Figure S2 of the Supporting Information). Plasmid DNA from selected clones with an N-terminal hexahistidine tag was isolated and transformed into *E. coli* M15 (pREP4) cells for protein expression.[15]

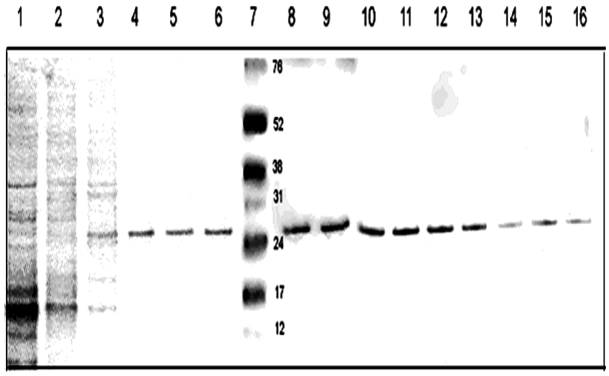

Figure 1. Tris-tricine SDS−PAGE showing the purification profile of Ace: lane 1, loading flow through; lane 2, wash 1; lane 3, wash 2; lane 7, protein molecular weight marker; lanes 4−6 and lanes 8−16, elution fractions.

Expression of Ace was induced by the addition of 0.5 mM isopropyl β-D-thiogalactopyranoside (IPTG) to an *E. coli* M15 (pREP4) cell culture with an OD_{595} of 0.3, for 4 h at 37 °C. Cells were harvested and resuspended in sonication buffer [50 mM potassium phosphate, 300 mM potassium chloride, and 5% glycerol (pH 8.0)], sonicated, and centrifuged. The protein obtained in supernatant was loaded into a pre-equilibrated nickel agarose resin (Qiagen), which had been equilibrated in sonication buffer and washed sequentially with wash buffers containing 5, 10, and 15 mM imidazole. The protein was finally eluted in 20 mM imidazole-containing buffer, and the purity of the protein was checked on a 10% tris-tricine electrophoresis gel under denaturing conditions. Because Ace is an acidic protein (pI 4.26), it did not stain with standard Coomassie blue staining; silver nitrate staining was conducted according to the standard protocol[7] (Figure 1). Protein concentrations were estimated by the spectrophotometric method using an extinction coefficient of 26470 M^{-1} cm^{-1} (corresponding to one subunit of the protein) at 280 nm, as provided by the ExPASy Proteomics server (http://expasy.org/sprot/).

Fluorescence Measurements. Fluorescence spectra were recorded with a Jasco FP-750 spectrofluorometer (Jasco Ltd., Essex, U.K.) at a scan speed of 120 nm min^{-1} using a 1 cm path length quartz cuvette. Slit widths with a nominal band-pass of 5 nm were used for both excitation and emission. Intrinsic fluorescence emission spectra of Ace were recorded from 310 to 420 nm using 0.1 M potassium phosphate buffer (pH 8.0). An excitation wavelength of 295 nm was used to follow tryptophan fluorescence. The emission spectra of Ace were corrected for the buffer blank. The wavelengths at maximal emission intensity (λ_{max}) were determined.

Binding of bis-ANS to Ace was assessed at 25 °C using excitation at 395 nm using slit widths of 5 nm and measuring the emission fluorescence spectra between 420 and 600 nm. bis-ANS was added to 5 μM Ace, and the changes in ANS fluorescence were followed by measuring the intensity at 495 nm. For energy transfer experiments, an excitation wavelength of 295 nm was used to selectively excite tryptophan residues.

The solvent accessibility of tryptophan residues of Ace was determined using a fluorescence quenching method. Experiments were performed via addition of two different quenchers, potassium iodide and acrylamide, in 0.01 M increments to 5 μM

protein. Similar measurements were also taken using the protein denatured with 6 M GdnHCl.

Circular Dichroism Spectroscopy. Ellipticity was measured using a JASCO J800 spectropolarimeter equipped with a thermoelectrically controlled cell holder. A cuvette with a path length of 1 mm was employed for far-UV CD measurement, and spectra were recorded in the range of 200−260 nm, with a step resolution of 0.1 nm, a scan speed of 50 nm/min, and a bandwidth of 1 nm. A protein concentration of 10 μM was used with 0.1 M potassium phosphate buffer (pH 8.0), and each spectrum was averaged over three scans. For thermal unfolding of Ace, far-UV CD spectra were recorded as a function of temperature between 20 and 70 °C in steps of 2 °C with an equilibration time of 2 min at each temperature. The observed ellipticities were converted into the mean residue ellipticities ($[\theta]$) on the basis of a mean molecular mass per residue of 112 Da. The data were corrected for the baseline contribution of the buffer, and the observed ellipticities at 222 nm were recorded. The temperature dependence of the secondary structure was estimated from fitted far-UV CD curves.

Binding of Virstatin with Ace. A stock solution of virstatin was prepared by dissolving 5 mg of solid virstatin in DMSO. Binding of virstatin to Ace was studied by quenching of the typtophan fluorescence of protein as a probe. Virstatin-induced fluorescence quenching of Ace was monitored at 340 nm after the protein had been excited at 295 nm. The fluorescence quenching data of Ace induced by virstatin binding were presented as a plot of F_0/F_c versus virstatin concentration and were analyzed according to the Stern−Volmer equation.

Glutaraldehyde Cross-Linking. Because native Ace exists as a dimer, the oligomeric status of Ace after binding of virstatin was checked by a glutaraldehyde cross-linking experiment. Twenty micrograms of Ace was incubated with varying proportions of virstatin and then treated with 0.2 and 2.0% glutaraldehyde at room temperature for different periods of time. The reaction was then terminated by the addition of 200 mM glycine and 5× gel loading buffer. The samples were loaded on a 10% Tris-glycine SDS−PAGE gel along with a protein molecular weight marker from Fermentas. The bands were subjected to densitometry analysis to determine the dimer:tetramer ratio.

Cell Culture for the Activity Assay of Ace. Methods for maintenance of T84 cells in culture were described previously.[16] Briefly, T84 cells were grown in Dulbecco's modified Eagle's/F-12 medium (DMEM/F12, Mediatech Inc.) supplemented with 5% newborn calf serum. For Ussing chamber/voltage clamp experiments, 5×10^5 cells were seeded onto a 12 mm transwell insert (Costar 3407) and cultured for ∼12 days. The formation of a confluent layer of cells was ascertained by measuring the transepithelial electrical resistance with an EVOM Epithelial Voltohmmeter (WPI Inc., Sarasota, FL). When grown on polycarbonated filters, T84 cells are known to acquire the polarized phenotype of native colonic epithelia. The monolayers were refed the day before the experiments.

Transepithelial Cl^- Transport in Intact T84 Monolayers. T84 cells grown to confluence with resistance in the range of 1500−3000 Ω cm^2 were mounted in Ussing chambers and bathed with oxygenated (95% O_2/5% CO_2) HCO_3^-/Cl^- Ringer's solution at 37 °C. The Ringer's solution contained 115 mM NaCl, 25 mM $NaHCO_3$, 2.4 mM K_2HPO_4, 1.2 mM $CaCl_2$, 1.2 mM $MgCl_2$, 0.4 mM KH_2PO_4, and 10 mM glucose (pH 7.4). Five milliliters of Ringer's solution in each chamber was connected via KCl agar bridge to voltage and current electrodes described in ref 16. Monolayers were voltage-clamped to zero potential difference by the application of short-circuit current (I_{sc}) in a VCC MC6 multichannel voltage-current clamp amplifier (Physiologic Instruments Inc.). Under these conditions, changes in short-circuit current I_{sc} (ΔI_{sc}) in response to agonists are wholly reflective of electrogenic chloride (Cl^-) secretion.[17]

Antibacterial Assay. Bacterial strains *P. aeruginosa* MTCC 424, *Pr. mirabilis* MTCC 425, *S. aureus* MTCC 3160, and *E. coli* K12 were used for assaying the antibacterial activity of Ace. A culture of each strain saturated overnight in Growth Media 3 as specified from MTCC (1.0 g of beef extract, 2.0 g of yeast extract, 5.0 g of peptone, and 5.0 g of NaCl for 1.0 L) was inoculated into fresh medium and grown at 37 °C until the OD_{595} reached 0.5. The cells were harvested and washed with 10 mM sodium phosphate (pH 7.4). Cells were diluted in media such that a final cell density of $\sim 10^3$ cfu/mL is maintained per assay sample. Strains were incubated with increasing concentrations of Ace protein (0, 50, 100, and 200 μg/mL), each in triplicate in a 96-well tissue culture plate under aseptic conditions. The plate was incubated at 37 °C for 16 h in an incubator. The cell viability assay was determined spectrophotometrically by measuring the cell OD_{595} of each sample using a microplate reader.

Homology Modeling and Data Analysis. The primary sequence of Ace protein (Swiss-Prot entry C3M620-1) was obtained from SWISSPROT (http://expasy.org/sprot/). A BLAST search (http://blast.ncbi.nlm.nih.gov/Blast.cgi) with this sequence picked up approximately a dozen sequences, mostly close homologues of this enterotoxin, but none with known three-dimensional structure. Secondary structure prediction using PSIPRED (http://bioinf.cs.ucl.ac.uk/psipred/) indicated that the structure is mostly helical.[18] On-line servers provided structural models (data not shown) with helical content (∼70−80%) much in excess of the experimental values (∼40%). As such, we searched the SCOP database[19] (http://scop.mrc-lmb.cam.ac.uk/scop/) for toxins in the all-α category. All these toxins were individually aligned with the Ace sequence. All the sequences that aligned with minimal gaps and a high degree of sequence similarity were used as templates. The models obtained were analyzed to see if they tallied with the accessibility of the Trp residues as indicated by fluorescence experiments, and the secondary structure content suggested by CD data. The best template was found to be zhaoermiatoxin from *Zhaoermia mangshanensis* [Protein Data Bank (PDB) entry 2PH4],[20] which also happens to be a dimeric molecule as found in the case of Ace. Alignments between Ace and the template sequences were conducted using CLUSTALW;[21] the one between Ace and zhaoermiatoxin has the highest degree of sequence similarity (45%) and hence was used for modeling using MODELER version 6.0.[22] The stereochemical quality of the model was evaluated with PROCHECK[23] and WHATIF.[24] Secondary structures of the final three-dimensional model were calculated with DSSP,[25] and the solvent accessibility of the amino acids was calculated with NACCESS.[26] The modeled structure of Ace was then docked with virstatin using a docking server PATCHDOCK[27] and another program, GOLD.[28,29] Hydrogen bonding was then checked between the protein and the ligand using HBPLUS.[30]

RESULTS AND DISCUSSION

Characterization of Ace was hampered previously because of its low yield; an earlier attempt to clone *ace* into *E. coli* was not successful because of cell lysis, and hence Ace was purified from methylotrophic yeast *Pichia pastoris*.[7] In this study, Ace is purified

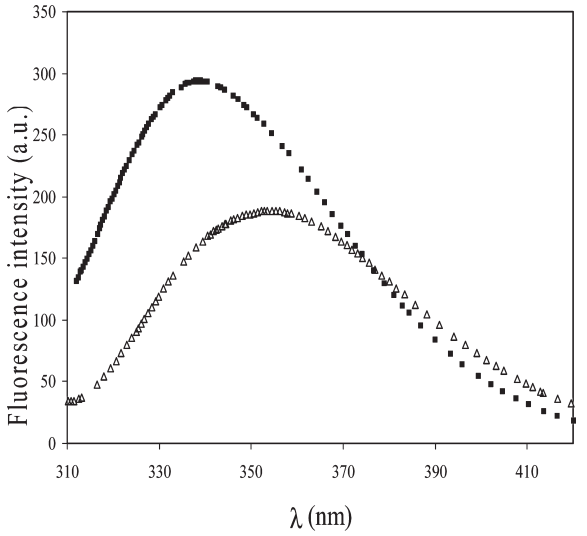

Figure 2. Fluorescence spectra of native Ace (λ_{ex} = 295 nm) (■) and Ace in the presence of 6 M GdnHCl (△).

from *E. coli* M15 (pREP4) cells with a quite good yield (0.8 g/L) for conducting various biophysical experiments. The purified protein exists in the dimeric form (Figure 1). As reported previously,[7] denaturing agent could not be used in the sample buffer because of the insolubility of the protein, and this precluded the appearance of any band due to the monomer.

Tryptophan Fluorescence Spectra of Ace. Tryptophan emission is quite sensitive to the polarity of the surrounding environment and is a useful probe of the local and overall conformation of proteins. When the sample is exposed to a more polar environment, the tryptophan emission maximum is red-shifted because of the hydrogen bonding interactions involving the indole nitrogen.[31,32] Native Ace has a tryptophan fluorescence emission maximum at 340 nm (Figure 2) and undergoes a progressive red shift with increasing concentrations of GdnHCl. For the unfolded Ace in the presence of 6 M GdnHCl, the emission intensity decreased, the maximum occurring at 353 nm, indicating the full exposure of tryptophan residues to the solvent.

Conformational Stability of Ace and Analysis of the Unfolding Data. To assess the stability of the protein, we studied the unfolding pathway of Ace using guanidinium hydrochloride (GdnHCl) and monitored it by fluorescence λ_{max} (λ_{ex} = 295 nm), as a function of denaturant concentration. Analysis of denaturant-induced unfolding curves of Ace followed a simple two-state transition between the folded (N) and unfolded (U) states. At each GdnHCl concentration, the observed signal *S*, representing the shift of the fluorescence emission maxima, was fit to a two-state equation as shown below

$$S = \frac{S_N e^{\Delta G_{NU}/(RT)} + S_U}{e^{\Delta G_{NU}/(RT)} + 1} \quad (1)$$

The plots of ΔG_{NU} (unfolding free energy) versus GdnHCl concentration were analyzed by linear least-squares analysis, according to the two-state model, by using the equation

$$\Delta G_{NU} = \Delta G_{NU}^{H_2O} - m_{NU}[d_{NU}]_{1/2} \quad (2)$$

where m_{NU} is the dependence of ΔG_{NU} on GdnHCl concentration, which is a measure of the cooperativity of unfolding, and $\Delta G_{NU}^{H_2O}$ is the free energy change in the absence of denaturant, which is

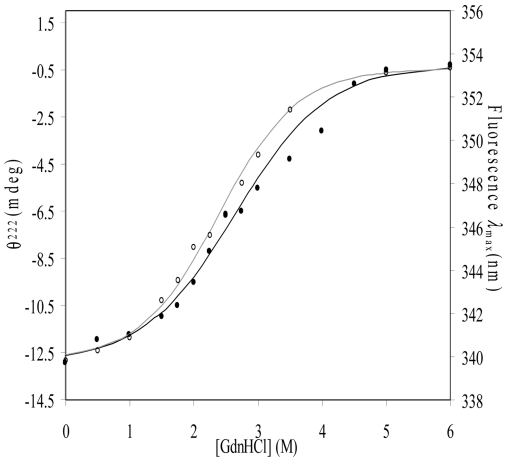

Figure 3. Unfolding of Ace using GdnHCl. Fluorescence λ_{max} (○) and ellipticity at 222 nm (●) overlaid along with the best fit curves assuming a two-state model.

Table 1. Two-State Analysis of Unfolding of Ace Using GdnHCl[a]

	λ_{max}-monitored value	CD-monitored value
S_N	340.1 ± 0.7	−12.6 ± 1.0
S_U	353.3 ± 0.3	−0.408 ± 1.00
ΔG_{NU} (kcal mol^{-1})	2.3 ± 0.4	2.2 ± 0.4
m_{NU} (kcal mol^{-1} M^{-1})	1.0 ± 0.2	0.8 ± 0.1
$[d_{NU}]_{1/2}$ (M)	2.4	2.7

[a] Based on data shown in Figure 3. Values listed are the average and standard deviation from four experimental measurements.

equivalent to the conformational stability of the protein. Dividing ΔG_{NU} by the slope gives the value for the midpoint of the transition, $[d_{NU}]_{1/2}$, as shown in eq 2.

To understand the conformational stability of the overall secondary structures of the protein, we also studied equilibrium unfolding of Ace by monitoring the far-UV CD (θ_{222}) in the presence of varying concentrations of GdnHCl (Figure 3). Addition of 6 M GdnHCl completely abolished the CD signal at 222 nm, indicating extensive or complete unfolding of Ace (Figure S3 of the Supporting Information). The unfolding free energies, calculated using eq 1, are listed in Table 1. The free energy of unfolding of the native Ace (ΔG_{NU}) is rather modest at 2.2 kcal mol^{-1}, whereas the value of the midpoint of the transition ($[d_{NU}]_{1/2}$) is 2.7 M. Very similar values are obtained when the unfolding transition is monitored using fluorescence λ_{max}.

Interaction of bis-ANS with Ace and the Transfer of Fluorescence Energy from Tryptophan to Bound bis-ANS. bis-ANS has been widely used as a fluorescent probe to monitor conformational changes in proteins and to determine the accessibility of hydrophobic surfaces.[10,11] Intrinsic fluorescence emission of bis-ANS increased with the addition of Ace, characteristic of bis-ANS binding to the hydrophobic region of Ace (Figure 4a).

Fluorescence energy transfer is a useful experimental approach for determining not only the proximity of different domains of a protein but also the binding affinity of probes for the protein.[33,34] Overlap of the tryptophan emission spectrum of Ace with the excitation spectrum of bis-ANS was manifest in the transfer of energy from the donor (tryptophan) to the acceptor (bis-ANS)

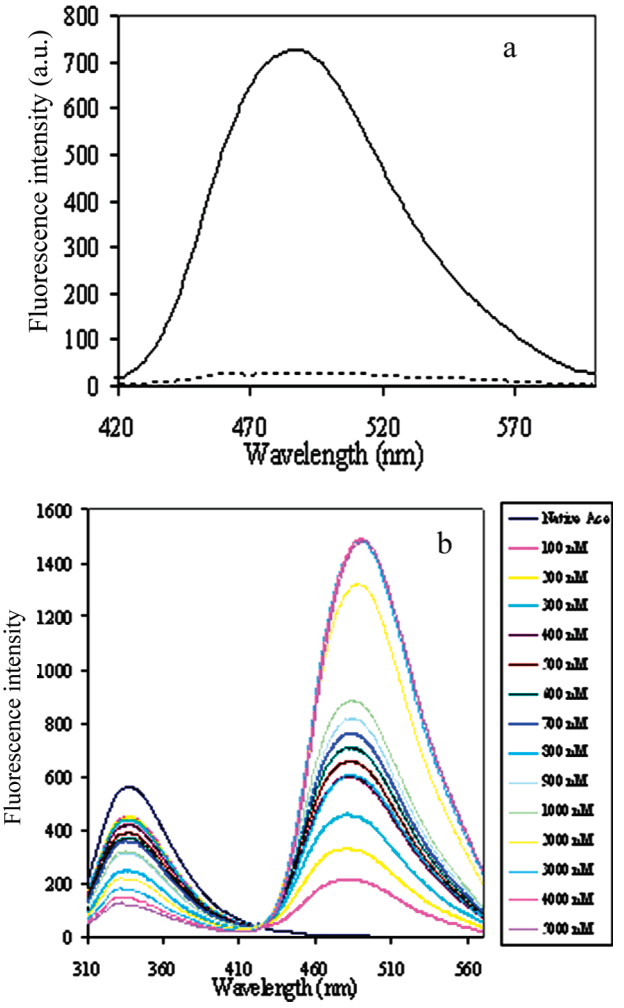

Figure 4. Fluorescence of Ace in the presence of bis-ANS. (a) Fluorescence spectra for bis-ANS alone (---) and in the presence of Ace (—) after excitation at 395 nm. (b) Transfer of energy between tryptophan in Ace and bound bis-ANS after excitation at 295 nm.

fluorophore (Figure 4b). Without bis-ANS, tryptophan residues of Ace emitted maximally at 340 nm. The addition of bis-ANS to the protein sample caused a decrease in tryptophan fluorescence at 340 nm coincident with the appearance of the dye fluorescence at 495 nm. Because an aqueous solution of free bis-ANS does not exhibit fluorescence upon excitation at 295 nm, we conclude that the 495 nm emission is entirely from bis-ANS that has bound to Ace.

Titration of bis-ANS Binding Sites in Ace. Titration of Ace with bis-ANS revealed exponential binding of the dye (Figure 5). The binding constant was calculated following the Hill model. The equation is

$$F_{obs} = F_{max}\frac{[\text{bis-ANS}]^n}{K' + [\text{bis-ANS}]^n} \quad (3)$$

where F_{obs} is the fluorescence intensity observed at a defined bis-ANS concentration, F_{max} is the maximal fluorescence intensity observed with a defined amount of protein, and the concentration of the dye is [bis-ANS]. The Hill coefficient n in eq 3 represents the number of bis-ANS binding sites on the protein, and K' is the apparent binding constant. In this study, the fluorescence

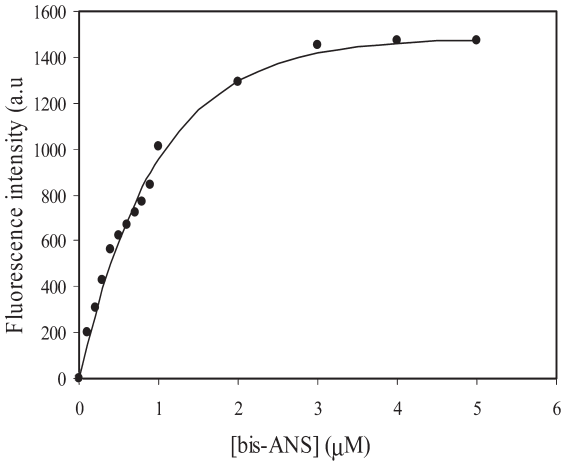

Figure 5. Titration of Ace (5 μM) with bis-ANS (0−5000 nM). The samples were excited at 395 nm, and the emission at 495 nm was measured.

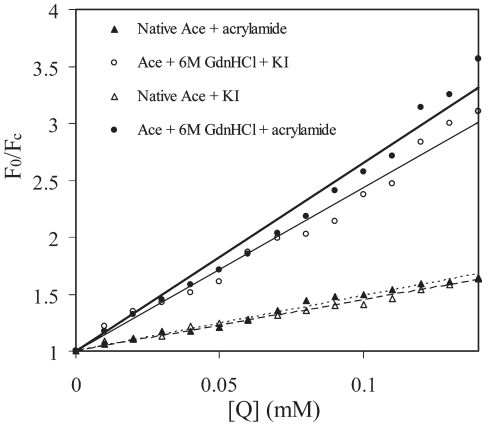

Figure 6. Stern−Volmer plots for quenching of tryptophan fluorescence of Ace (native form and that treated with 6 M GdnHCl) in the presence of quenchers (KI and acrylamide).

data were least-squares fitted to the Hill equation, yielding a binding constant K' of 0.72 μM and a Hill coefficient (n) of 0.98.

Quenching of the Tryptophan Fluorescence of Ace. Fluorescence quenching is the decrease in the fluorescence quantum yield of a fluorophore caused by a variety of molecular interactions such as excited state reactions, energy transfer, molecular rearrangement, formation of a nonfluorescent ground state complex (static quenching), and collisional encounter between the fluorophore and quencher (dynamic quenching).[35,36] Quenching was quantified using the Stern−Volmer equation to obtain the quenching constant, and the experimental data were fitted with the equation

$$\frac{F_0}{F_c} = 1 + K_{SV}[Q] \quad (4a)$$

where F_0 is the fluorescence without a quencher, F_c is the fluorescence in the presence of a given quencher concentration [Q], and K_{SV} is the Stern−Volmer constant. The values of K_{SV} obtained from the slope of the linear plot for native Ace (Figure 6) are 4.87 and 4.45 M^{-1} for acrylamide and KI, respectively. In the presence of 6 M GdnHCl, the protein unfolds, resulting in the

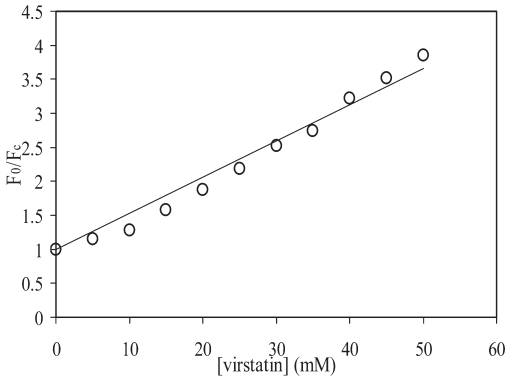

Figure 7. Stern−Volmer plot for the quenching for Ace using virstatin.

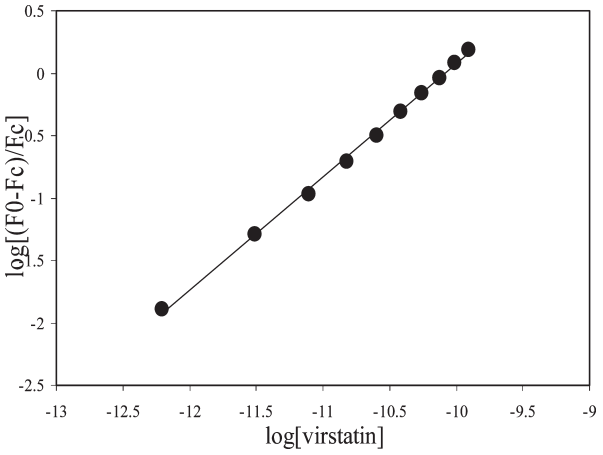

Figure 8. Plot of $\log[(F_0 - F_c)/F_c]$ vs log[virstatin] for the fluorescence quenching of Ace with virstatin.

exposure of all the Trp residues to the solvent, which become more accessible to both the quenchers, and this is evident from the higher values of K_{SV} (16.54 and 14.32 M^{-1} for acrylamide and KI, respectively).

Iodide (ionic) usually quenches tryptophan(s) at or near the surface, while acrylamide (nonionic) could quench tryptophan(s) near the surface and could quench tryptophan(s) in the hydrophobic interior of the protein through diffusion. As KI and acrylamide give a similar quenching effect for native Ace, it is likely that all four Trp residues (W10, W17, W26, and W38) are exposed, or even if one or more Trp residues are buried, acrylamide is not able to diffuse into these locations. The fraction of total fluorophore accessible to the quencher can be calculated from the modified Stern−Volmer plot, also known as the Lehrer plot.

$$\frac{F_0}{F_0 - F_c} = \frac{1}{f_A} + \frac{1}{K_{SV} f_A [Q]} \quad (4b)$$

where f_A is the fraction of the initial fluorescence, which is accessible to the quencher. The Lehrer plots for the two quenchers (Figure S4 of the Supporting Information) show some deviation from linearity, indicating the possibility of the existence of at least two types of populations of Trp residues. The percentages of the total fluorescence quenched by these quenchers calculated using eq 4b were found to be 67 and 84% for acrylamide and KI, respectively. This suggests that approximately three of four Trp residues are exposed to the solvent. This has also been validated by the structural model of Ace (discussed later).

Interaction of Virstatin with Ace and Determination of Binding Constants. Fluorescence quenching of protein could be used to derive protein−drug binding information.[37−39] Static quenching is caused by the formation of a nonfluorescent ground state fluorophore−quencher complex. Fluorescence quenching of Ace by virstatin was monitored at 340 nm after the protein had been excited at 295 nm. The data for the fluorescence quenching of Ace induced by virstatin are presented as a Stern−Volmer plot as F_0/F_c versus virstatin concentration (Figure 7), and the quenching data are analyzed with eq 4a.

The binding constant for the Ace−virstatin complex was determined, as reported for several protein−drug complexes.[40] If there are n substantive binding sites on the surface of protein to accommodate the ligand molecules, the equilibrium between the free and bound molecule is given by

$$\log\left(\frac{F_0 - F_c}{F_c}\right) = \log(K) + n \log[Q] \quad (5)$$

where F_0, F_c, and [Q] are the same as the parameters in the Stern−Volmer equation. K is the binding constant.

A plot of $\log[(F_0 - F_c)/F_c]$ versus log([Q]) gave a straight line using least-squares analysis for the Ace−virstatin interaction (Figure 8). The linearity in the plot of $\log[(F_0 - F_c)/F_c]$ versus virstatin concentration log[Q] suggests the existence of one type of binding site, and the slope of the plot led to the determination of the binding capacity ($n = 0.9$). The intercept on the Y axis gave the value of the binding constant (9×10^4 M^{-1}), which was used to calculate the standard free energy change ($\Delta G°$) from the relationship[41]

$$\Delta G° = -2.303RT \log(K) \quad (6)$$

The value of the free energy change was found to be 12 kcal mol^{-1}.

Effect of Virstatin Binding on the Conformation of Ace. Circular dichroism (CD) is one of the strong and sensitive spectroscopic techniques that provides a global measure of the secondary structural features present in a protein and also during its interaction with small molecules.[42,43] In recent years, the development of deconvolution algorithms and the general availability of CD spectral databases have allowed an accurate determination of secondary structure prediction of proteins.[44] To study the influence of virstatin on the secondary structure of Ace, the far-UV CD (200−260 nm) spectra were recorded at various drug:protein molar ratios (0, 1:1, 2:1, and 3:1). During CD measurements, the DMSO (used as a solvent for the ligand) content never exceeded 1.5% (v/v). Figure 9 shows the far-UV CD spectra of Ace in the absence and presence of the ligand at different molar ratios. The decrease in the magnitude of the signal at 222 nm was indicative of destabilization of helical structure upon binding to virstatin. Deconvolution analysis of the CD spectra by the neural network method using CDNN[45] showed that native Ace contains 40% α-helix (Table S1 of the Supporting Information). When virstatin was incubated with Ace at a 1:1 molar ratio, the α-helical content of Ace was reduced to 30% with a concomitant increase in random coil content. With a further increase in the concentration of the ligand (1:2 and 1:3 Ace:virstatin molar ratios), the secondary structure of Ace was further reduced, indicative of a partial unfolding of the protein in the presence of the drug.

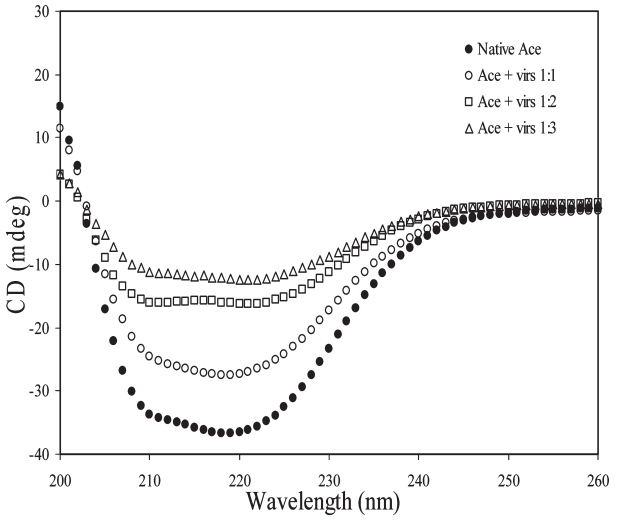

Figure 9. Far-UV CD spectra of Ace in the presence of virstatin, at Ace: virstatin molar ratios of 1:1, 1:2, and 1:3.

Thermal Stability of Ace in the Presence or Absence of Virstatin. The changes in CD as a function of temperature, at characteristic wavelengths, can be used to determine the thermodynamics of unfolding.[46] Temperature-dependent CD profiles of Ace protein, as well as Ace in presence of virstatin (1:1 molar ratio), have been recorded at 222 nm to selectively monitor the disruption of secondary structure. Results are reported in terms of the mean residue ellipticity ($[\theta]$, degrees square centimeters per decimole), which is given by

$$[\theta_{222}] = (100\theta M_W)/(clN) \quad (7)$$

where $[\theta_{222}]$ is the measured ellipticity in degrees, c is the protein concentration in milligrams per milliliter, l is the path length in centimeters, and M_W and N are the molecular weight of and the number of amino acid residues in Ace, respectively. Considering that the unfolding of the Ace is a two-state process between folded state F and unfolded state U, the equilibrium constant K at any temperature T can be written as

$$K = \frac{[F]}{[U]} \quad (8)$$

where [F] and [U] are the concentrations of the folded and unfolded forms, respectively. The equilibrium constant K is related to the Gibbs free energy of unfolding as

$$\Delta G = -RT \ln K \quad (9)$$

where R is the gas constant and T is the absolute temperature.

Again the fraction folded at any temperature α is given by

$$\alpha = \frac{[F]}{[F] + [U]} \quad (10)$$

which is $K/(1 + K)$ and

$$\alpha = \frac{\theta_T - \theta_U}{\theta_F - \theta_U} \quad (11)$$

where θ_T is the observed ellipticity at any temperature T, θ_F is the ellipticity of the fully folded form, and θ_U is the ellipticity of the unfolded form. To fit the change of CD at a single wavelength as a function of temperature T, we used the Gibbs−Helmholtz equation.

$$\Delta G = \Delta H(1 - T/T_M) - \Delta C_p T_M[1 - T/T_M + (T/T_M) \ln(T/T_M)] \quad (12)$$

where T_M is the melting temperature, ΔH is the change in enthalpy, and ΔC_p is the change is specific heat capacity from the folded to the unfolded state. The midpoints of the unfolding transition T_M, determined from the sigmoidal fits to the plot of $[\theta_{222}]$ with temperature, were found to be 53.4 and 51.5 °C for native Ace and Ace treated with virstatin, respectively. Analysis of the thermal unfolding curves (Figure S5 of the Supporting Information) showed that the midpoint temperature (T_M) of native Ace was slightly greater compared to that of virstatin-treated Ace, indicating a higher thermal stability of the native protein.

Oligomeric Status of Ace in the Presence of Virstatin. The purified Ace exists predominantly in the dimeric form (Figure 1), and we studied the effect of virstain on its oligomeric state. Glutaraldehyde-cross-linked Ace showed the presence of ∼55% tetramer (lane 2 of Figure S6 of the Supporting Information), while samples containing 1:1 (lane 3) and 1:5 (lane 4) protein: virstatin ratios showed 50 and 45% tetramerization, respectively. An increase in the concentration of glutaraldehyde or the incubation time (lanes 6−10) augmented the tetrameriztion and the formation of higher-order oligomers. So in contrast to its disruption of dimerization of ToxT, [47] virstatin did not significantly affect the oligomerization of Ace. Though the SDS−PAGE results from our study and earlier studies[7] show the existence of the dimeric form, on reaction with glutaraldehyde (a short cross-linker with a non-zero length), the higher-order oligomers also appear. The fact that oligomers like trimer, pentamer, hexamer, etc., did not appear on cross-linking indicates that the observed oligomeric forms are not due to nonspecific intermolecular interactions. It has previously been hypothesized that the amphipathic 20-amino acid, C-terminal end of Ace may play some role in the formation and insertion of the Ace multimer into the eukaryotic membrane as in some family of ion-transporting ATPases.[5] Though the dimeric form of Ace is the most prevalent form, the occurrence of the tetramer and octamer in presence of glutaraldehyde may indicate that the higher-order oligomeric forms may also be biologically relevant.

Biological Activity of Recombinant Ace. To determine whether purified Ace is biologically active, we measured I_{sc} in T84 monolayers after apical addition of Ace to the Ussing chamber. Purified Ace alone did not alter I_{sc}. However, it induced a dose-dependent increase in the I_{sc} across T84 monolayers along with ATP stimulation (Figure 10a). The maximal effect on I_{sc} was found with 1 μM purified Ace on the apical side (130 ± 10 μA/cm^2) when compared with ATP alone (45 ± 7 μA/cm^2). This response was significantly inhibited by bumetanide (32.31 ± 8 μA/cm^2; $P < 0.001$), an inhibitor of the Na,K,Cl-cotransporter, indicating that this current is carried (predominantly) by Cl^- (Figure 10c).

Ace has previously been shown to stimulate secretion of Cl^- across intestinal epithelial cells; however, the effects of Ace on ATP-dependent Cl^- secretion have not been investigated previously. We initially set out to determine whether purified Ace is biologically active and thus enhances the ability of epithelial cells to transport Cl^- in response to a calcium-dependent stimulus. The purinergic agonist ATP was used as a prototypic receptor-mediated calcium-dependent secretagogue. The Cl^- secretory response to ATP, expressed as the change in I_{sc}, was potentiated by pretreatment of Ace in a dose-dependent fashion. This

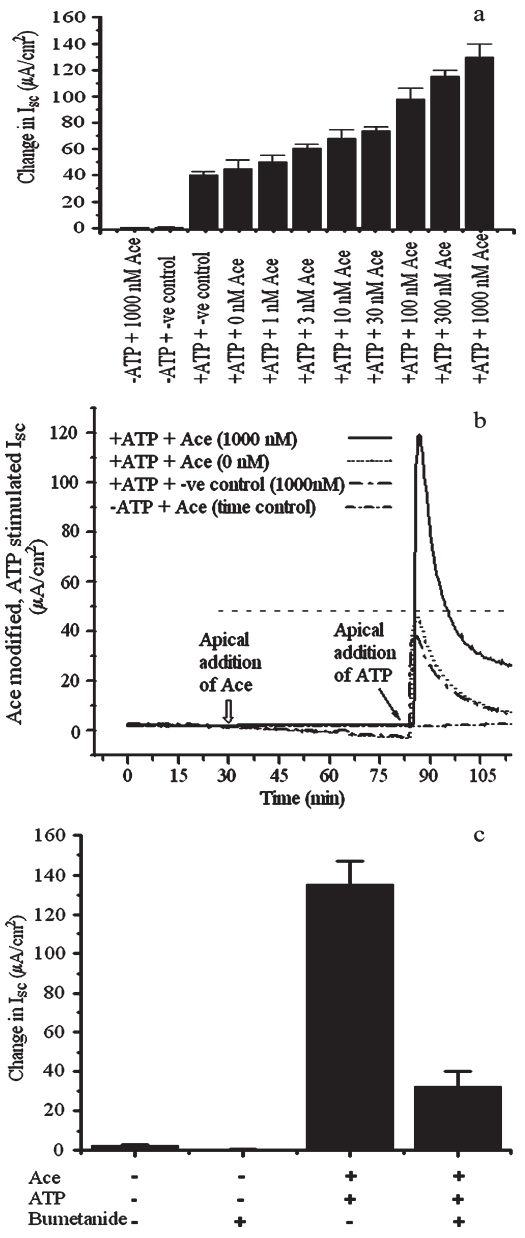

Figure 10. Effect of different concentrations of Ace (as indicated, in nanomolar) on Cl^- secretion over ATP (100 μM) stimulation in human intestinal epithelial cells (T84). Short-circuit current (I_{sc}) was used to measure current produced by secreted Cl^-. (a) Summary of dose−response data (mean ± standard error; n = 4). The change in I_{sc} was derived from the I_{sc} value before and after addition of either Ace, ATP alone, or Ace with ATP (P < 0.002). (b) Representative real-time traces of Isc measurement in T84 cells presented in panel a. The horizontal dotted line demonstrates that Ace significantly potentiated Cl^- secretion over ATP stimulation. After equilibration for 30 min, cells were preincubated with different concentrations of apical Ace (open arrow); thereafter, ATP (↓) was added on the apical side, and I_{sc} was recorded. (c) Ace-modified ATP-stimulated Cl^- secretion measured in T84 cells preincubated with basolateral bumetanide (100 μM) for 30 min. Bumetanide significantly reduced the level of Cl^- secretion (P < 0.001; values are means ± standard error; n = 3). Statistical analyses were performed using t-test by the statistical software Origin (version 6.0). P < 0.05 was considered significant.

synergistic response of secretion of Cl^- by Ace and ATP was surprising and intriguing because Ace alone did not have any

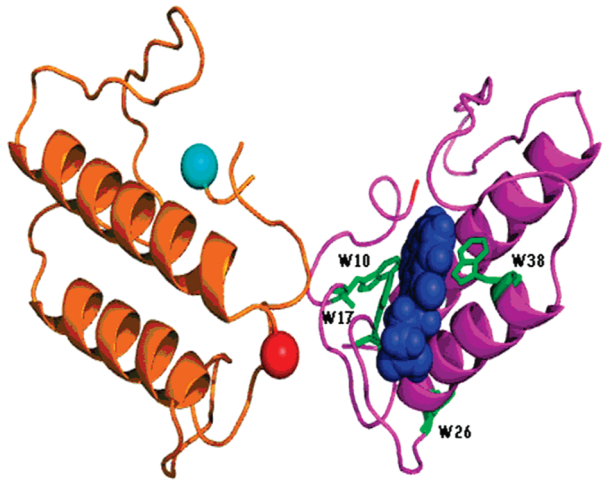

Figure 11. Model of Ace with bound virstatin. Dimeric Ace protein docked with one molecule of virstatin (blue), with four tryptophan residues (green). The N- and C-terminal ends are represented as cyan and red spheres, respectively.

effect on I_{sc} change but its pretreatment was just robust and transient. These effects may occur via another mechanism of Cl^- transport in the cells that was not assessed in this study. It is possible that Ace may have effects on the cells other than those directly associated with an increase in the cytosolic calcium level; otherwise, Ace alone would increase I_{sc} as ATP alone did (Figure 10b). The basis for their synergistic action remains to be fully elucidated in determining whether interaction at the level of the transport pathway activated by Ace along with ATP could explain the synergistic action.

Structural Model of Ace. Among the potential template structures, zhaoermiatoxin from *Zhaoermia mangshanensis* (PDB entry 2PH4) was selected for homology modeling because of some similarity of function and considerable sequence similarity (45%) to the query (Figure S7 of the Supporting Information) compared to the others. Stereochemical evaluation of backbone ϕ and ψ dihedral angles by PROCHECK revealed that 83.9, 10.9, 4.1, and 1.1% of residues were within the most favored region, additionally allowed region, generously allowed region, and disallowed region, respectively, of the Ramachandran plot. Similarly, WHATIF revealed that the root-mean-square Z score for bond lengths, root-mean-square Z score for bond angles, ω angle restraints, side chain planarity, improper dihedral distribution, and outside distribution were 0.912, 1.368, 0.760, 0.407, 0.999, and 1.351, respectively for the modeled structure, which are all positive values (positive is better than average).

Swiss-Prot annotation shows that Ace has a potential transmembrane helical region at the C-terminal end (residues 76−96), but because there is a long gap in the alignment after position 87 (Figure S7 of the Supporting Information), modeling was not performed beyond this position. It has been suggested that the 20-residue C-terminal end of the chain has an amphipathic character and could be useful for the insertion of Ace multimers into the eukaryotic membrane.[5] It is possible that the missing residues in the model could form helical structure protruding vertically down from the C-terminal end of the structure shown in Figure 11. It may be mentioned that zhaoermiatoxin, on the basis of which Ace has been modeled, is a catalytically inactive, myotoxic Arg49 phopholipase A_2 homologue and has a well-ordered C-terminus, which in addition to

Table 2. Accessible Surface Areas (ASA) and Relative Accessibilities of Tryptophan Residues in Ace before and after Docking with Virstatin

	before		after	
residue	ASA (Å^2)	relative accessibility[a] (%)	ASA (Å^2)	relative accessibility[a] (%)
Trp10	2.1	0.8	2.1	0.8
Trp17	13.1	5.3	1.7	0.7
Trp26	188.6	75.7	188.6	75.7
Trp38	42.9	17.2	11.5	4.6

[a] Accessibility has been computed with NACCESS. Residues with relative accessibility of <5% may be considered buried.[57]

hydrophobic Phe residues at specific positions contains a number of positively charged Lys residues. These residues are implicated in membrane insertion, with the hydrophobic groups interacting with the hydrocarbon chains of phospholipids and the basic residues with the acidic polar headgroups.[20] Interestingly, Ace also contains Arg residues that align with the Lys residues in the C-terminal region.

The two subunits bury an interface area of 707 Å^2 between them. The modeled structure conforms to the experimental data derived from biophysical experiments. For example, the structure has a helical content of 38%, approximately the same as that inferred from the deconvolution of the CD data (Table S1 of the Supporting Information). Assuming a relative accessibility of <5% to identify buried residues, there is only one residue (Trp10) that is buried in the native ASA structure (Table 2).

Docking. Quite similar solutions were obtained from both docking programs, PATCHDOCK and GOLD. However, while the solution from PATCHDOCK showed no hydrogen bonds, the one from GOLD had three hydrogen bonds (two with Thr16 and one with Gln35) (Figure S8 of the Supporting Information) and has been considered for analysis (Figure 11). Consideration of the accessibility of Trp residues (Table 2) indicates that after docking with virstatin the accessible areas of Trp17 and Trp38 are reduced. Table S2 of the Supporting Information indicates that 86% of the surface area of virstatin is buried upon formation of the complex. Zhaoermiatoxin, a phospholipase A_2 homologue in which the catalytic Asp49 has been replaced with an Arg residue and is thus catalytically inactive, was used to model Ace. This structure also showed electron density (into which a fragment of a PEG-400 molecule could be fitted) in both subunits at the hydrophobic channel that leads to what otherwise would have been the active site.[20] This hydrophobic pocket is also the site of binding in Ace.

Antibacterial Assay. It has often been reported that microbially produced toxins may be antimicrobially significant to the producers.[48] For example, proteins from many subspecies of *Bacillus thuringiensis*, an insect pathogen, have been found to affect various representatives of *Micrococcus*, *Staphylococcus*, *Nocardia*, *Streptomyces*, *Erwinia*, etc.[49] Ace being an important endotoxin produced by *V. cholerae*, a human pathogen, made us search for any antimicrobial significance of the protein to its producer. Four different microbial strains, viz., *E. coli* K12, *S. aureus*, *P. aeruginosa*, and *Pr. mirabilis*, were grown in the presence of increasing concentrations of Ace (Figure 12). A decreased absorbance by the cells at 595 nm was observed with increasing concentrations of Ace; 200 μg/mL Ace seems to have significant antimicrobial activities with respect to all of the strains used for the experiment. The percentage cell killing was calculated to be ~75% for *E. coli* K12 and *P. aeruginosa* and 80 and 72% for *S. aureus* and *Pr. mirabilis*, respectively. Previous reports indicated

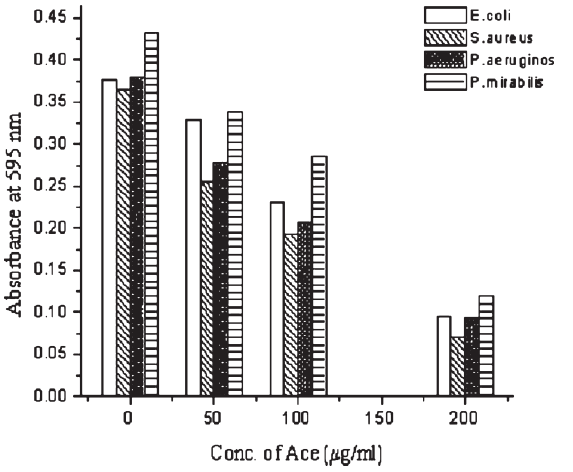

Figure 12. Toxicity assay of Ace vs various microorganisms. Bar diagrams indicate the absorbance at 595 nm for cells incubated with varying concentrations of Ace.

that Ace stimulates influx of Ca^{2+} through calcium channels followed by Cl^-/HCO_3^- secretion with the involvement of Na^+/K^+-ATPase, $Na^+/K^+/2Cl^-$ cotransporters (NKCC), and K^+ channels in a Ca^{2+} secondary messenger-dependent pathway in the eukaryotic host.[6] Whether these components are also involved in the antimicrobial effect of Ace is yet to be investigated. Phylogenetic studies reveal that the NKCC family of proteins, mostly characterized in the eukaryotes, has its roots in the prokaryotic kingdom.[50] The presence of EF-hand-type Ca^{2+}-binding proteins in various bacteria and their participation in a variety of cellular processes, including motility, chemotaxis, cell division, and differentiation, has been demonstrated.[51−53] The transport of calcium into and out of cells is immensely important for the survival of bacterial cells.[54,55] Details of the mechanism involved remain to be explored.

CONCLUSIONS

Recently, Ace and its analogues have been used to treat cystic fibrosis (CF), a common genetic disease among the Caucasian population.[56] CF involves insufficient chloride transport and subsequently leads to a loss of luminal sodium and water, which in turn causes epithelial and connective tissue damage resulting in bronchial distortion. Via the administration of Ace or its analogues, the level of secretion of chloride in the lungs increases with the concomitant increase in the amount of airway surface water in the lumen of the lungs. Therefore, from the medicinal point of view, it is important to understand its structure and

function. Here we have cloned and expressed the recombinant protein, and for a biological role, it could potentiate Cl^- secretion over ATP stimulation. This protein was used to conduct biophysical studies to elucidate its stability, Trp exposure, and the occurrence of hydrophobic surface patches in the structure. Virstatin has been shown to inhibit virulence regulation in *V. cholerae* by inhibiting the dimerization and thereby the function of the virulence transcription activator, ToxT.[47] Here we have shown that virstatin also binds Ace, and the binding, though it does not have any significant effect on the oligomeric status of the molecule, has a deleterious consequence on the secondary structure. This effect of virstatin on Ace may have an important connotation for its development as an antimicrobial. A homology model of Ace that shows the possible location of the binding site and involvement of Trp residues has been generated, as indicated by fluorescence studies.

■ ASSOCIATED CONTENT

Supporting Information. Effect of binding of virstatin on the conformation of Ace (Table S1), change in the accessibility of virstatin upon binding of Ace (Table S2), chemical structure of virstatin (Figure S1), DNA sequencing of the *ace* gene (Figure S2), far-UV CD spectra of native Ace and Ace in the presence of 6 M GdnHCl (Figure S3), Lehrer plots for Trp fluorescence quenching (Figure S4), variation of ellipticity at 222 nm with temperature for native Ace and Ace treated with virstatin (Figure S5), glutaraldehyde cross-linking of Ace and Ace treated with various concentrations of virstatin (Figure S6), alignment of the Ace sequence with the template zhaoermiatoxin (Figure S7), and LIGPLOT representation of the environment of the bound virstatin (Figure S8). This material is available free of charge via the Internet at http://pubs.acs.org.

■ AUTHOR INFORMATION

Corresponding Author

*E-mail: tanaya_chatterjee@yahoo.com (T.C.) or pinak@boseinst.ernet.in (P.C.). Telephone: +91-33-2569-3253. Fax: +91-33-2355-3886.

Funding Sources

T.C. is supported by a Young Scientist Grant from the Department of Science and Technology, Government of India, and P.C. by the J. C. Bose National Fellowship. D.M. was awarded a fellowship by the Council of Scientific and Industrial Research, Government of India, and S.D. a fellowship by the Department of Biotechnology, Government of India.

■ ACKNOWLEDGMENT

We thank Dr. Dipak Manna for discussion.

■ ABBREVIATIONS

SDS, sodium dodecyl sulfate; Ni-NTA, nickel nitriloacetic acid; PMSF, phenylmethanesulfonyl fluoride; DMSO, dimethyl sulfoxide; I_{sc}, short-circuit current.

■ REFERENCES

(1) Sears, C. L., and Kaper, J. B. (1996) Enteric bacterial toxins: Mechanisms of action and linkage to intestinal secretion. *Microbiol. Rev. 60*, 167–215.

(2) Gill, D. M., and Coburn, J. (1987) ADP-ribosylation by cholera toxin: Functional analysis of a cellular system that stimulates the enzymatic activity of cholera toxin fragment A1. *Biochemistry 26*, 311–316.

(3) Fasano, A., Baudry, B., Pumplin, D. W., Wasserman, S. S., Tall, B. D., Ketley, J. M., and Kaper, J. B. (1991) *Vibrio cholerae* produces a second enterotoxin, which affects intestinal tight junctions. *Proc. Natl. Acad. Sci. U.S.A. 88*, 5242–5246.

(4) Fasano, A., and Uzzau, S. (1997) Modulation of intestinal tight junctions by *Zonula occludens* toxin permits enteral administration of insulin and other macromolecules in an animal model. *J. Clin. Invest. 99*, 1158–1164.

(5) Trucksis, M., Galen, J. E., Michalski, J., Fasano, A., and Kaper, J. B. (1993) Accessory cholera enterotoxin (Ace), the third toxin of a *Vibrio cholerae* virulence cassette. *Proc. Natl. Acad. Sci. U.S.A. 90*, 5267–5271.

(6) Trucksis, M., Conn, T. L., Wasserman, S. S., and Sears, C. L. (2000) *Vibrio cholerae* ACE stimulates Ca^{2+}-dependent Cl^-/HCO_3^- secretion in T84 cells in vitro. *Am. J. Physiol. 279*, 567–577.

(7) Trucksis, M., Conn, T. L., Fasano, A., and Kaper, J. B. (1997) Production of *Vibrio cholerae* Accessory Cholera Enterotoxin (Ace) in the Yeast *Pichia pastoris*. *Infect. Immun. 65*, 4984–4988.

(8) Henkens, R. W., Kitchell, B. B., Lottich, S. C., Stein, P. J., and Williams, T. J. (1982) Detection and characterization using circular dichroism. *Biochemistry 21*, 5918–5923.

(9) Kelly, S. M., and Price, N. C. (1997) The application of circular dichroism to studies of protein folding and unfolding. *Biochim. Biophys. Acta 1338*, 161–185.

(10) Shi, L., Palleros, D. R., and Fink, A. L. (1994) Protein conformational changes induced by 1,19-bis(4-anilino-5-naphthalenesulfonic acid): Preferential binding to the molten globule of DnaK. *Biochemistry 33*, 7536–7546.

(11) Smoot, A. L., Panda, M., Brazil, B. T., Buckle, A. M., Fersht, A. R., and Horowitz, P. M. (2001) The binding of bis-ANS to the isolated GroEL apical domain fragment induces the formation of a folding intermediate with increased hydrophobic surface not observed in tetradecameric GroEL. *Biochemistry 40*, 4484–4492.

(12) Puri, A. W., and Bogyo, M. (2009) Using small molecules to dissect mechanisms of microbial pathogenesis. *ACS Chem. Biol. 4*, 603–616.

(13) Ong, S. E., Schenone, M., Margolin, A. A., Li, X., Do, K., Doud, M. K., Mani, D. R., Kuai, L., Wang, X., Wood, J. L., Tolliday, N. J., Koehler, A. N., Marcaurelle, L. A., Golub, T. R., Gould, R. J., Schreiber, S. L., and Carr, S. A. (2009) Identifying the proteins to which small-molecule probes and drugs bind in cells. *Proc. Natl. Acad. Sci. U.S.A. 106*, 4617–4622.

(14) Hung, D. T., Shakhnovich, E. A., Pierson, E., and Mekalanos, J. J. (2005) Small-molecule inhibitor of *Vibrio cholerae* virulence and intestinal colonization. *Science 310*, 670–674.

(15) Sambrook, J., Fritsch, E. F., and Maniatis, T. (1989) *Molecular cloning: A laboratory manual*, Cold Spring Harbor Laboratory Press, Plainview, NY.

(16) Hoque, K. M., Woodward, O. M., van Rossum, D. B., Zachos, N. C., Chen, L., Leung, G. P., Guggino, W. B., Guggino, S. E., and Tse, C. M. (2010) *J. Gen. Physiol. 135*, 43–58.

(17) Cartwright, C. A., McRoberts, J. A., Mandel, K. G., and Dharmsathaphorn, K. (1985) *J. Clin. Invest. 76*, 1837–1842.

(18) McGuffin, L. J., Bryson, K., and Jones, D. T. (2000) The PSIPRED protein structure prediction server. *Bioinformatics 16*, 404–405.

(19) Murzin, A. G., Brenner, S. E., Hubbard, T., and Chothia, C. (1995) SCOP: A structural classification of proteins database for the investigation of sequences and structures. *J. Mol. Biol. 247*, 536–540.

(20) Murakami, M. T., Kuch, U., Betzel, C., Mebs, D., and Arni, R. K. (2008) Crystal structure of a novel myotoxic Arg49 phospholipase A2 homolog (zhaoermiatoxin) from *Zhaoermia mangshanensis* snake venom: Insights into Arg49 coordination and the role of Lys122 in the polarization of the C-terminus. *Toxicon 51*, 723–735.

(21) Thompson, J. D., Higgins, D. G., and Gibson, T. J. (1994) CLUSTAL W: Improving the sensitivity of progressive multiple

sequence alignment through sequence weighting, position-specific gap penalties and weight matrix choice. *Nucleic Acids Res. 22*, 4673–4680.

(22) Fiser, A., and Sali, A. (2003) Modeller: Generation and refinement of homology-based protein structure models. *Methods Enzymol. 374*, 461–491.

(23) Laskowski, R. A., MacArthur, M. W., Moss, D. S., and Thornton, J. M. (1993) PROCHECK: A programme to check the stereochemical quality of protein structures. *J. Appl. Crystallogr. 26*, 283–291.

(24) Vriend, G. (1990) WHATIF: A molecular modelling and drug design program. *J. Mol. Graphics 8*, 52–56.

(25) Kabsch, W., and Sander, C. (1983) Dictionary of protein secondary structure: Pattern recognition of hydrogen-bonded and geometrical features. *Biopolymers 22*, 2577–2637.

(26) Hubbard, S. J. (1992) *NACCESS: Program for Calculating Accessibilities*, Department of Biochemistry and Molecular Biology, University College London, London.

(27) Schneidman-Duhovny, D., Inbar, Y., Nussinov, R., and Wolfson, H. J. (2005) PatchDock and SymmDock: Servers for rigid and symmetric docking. *Nucleic Acids Res. 33*, 363–367.

(28) Jones, G., Willett, P., Glen, R. C., Leach, A. R., and Taylor, R. (1997) Development and validation of a genetic algorithm for flexible docking. *J. Mol. Biol. 267*, 727–748.

(29) Jones, G., Willett, P., and Glen, R. C. (1995) Molecular recognition of receptor sites using a genetic algorithm with a description of desolvation. *J. Mol. Biol. 245*, 43–53.

(30) McDonald, I. K., and Thornton, J. M. (1994) Satisfying hydrogen bonding potential in proteins. *J. Mol. Biol. 238*, 777–793.

(31) Lakowicz, J. R. (1983) *Principles of fluorescence spectroscopy*, Plenum Press, New York.

(32) Bolen, D. W., and Santoro, M. M. (1988) Unfolding free energy changes determined by the linear extrapolation method. *Biochemistry 27*, 8069–8074.

(33) Bothra, A., Bhattacharyya, A., Mukhopadhyay, C., Bhattacharyya, K., and Roy, S. (1988) A fluorescence spectroscopic and molecular dynamics study of bis-ANS/protein interaction. *J. Biomol. Struct. Dyn. 15*, 959–966.

(34) Prasad, A. R., Luduena, R. F., and Horowitz, P. M. (1986) Detection of energy transfer between tryptophan residues in the tubulin molecule and bound bis(8-anilinonaphthalene-1-sulfonate), an inhibitor of microtubule assembly, that binds to a flexible region on tubulin. *Biochemistry 25*, 3536–3540.

(35) Eftink, M. R., and Ghiron, C. A. (1981) Fluorescence quenching studies with proteins. *Anal. Biochem. 114*, 199–227.

(36) Kandagal, P. B., Ashoka, S., Seetharamappa, J., Shaikh, S. M., Jadegoud, Y., and Ijare, O. B. (2006) Study of the interaction of an anticancer drug with human and bovine serum albumin: Spectroscopic approach. *J. Pharm. Biomed. Anal. 41*, 393–399.

(37) Ahmad, B., Parveen, S., and Khan, R. (2006) Effect of albumin conformation on the binding of ciprofloxacin to human serum albumin: A novel approach directly assigning binding site. *Biomacromolecules 7*, 1350–1356.

(38) Pace, C. N. (1990) Measuring and increasing protein stability. *Trends Biotechnol. 8*, 93–98.

(39) Cantor, C. R., and Schimmel, P. R. (1980) *Biophysical chemistry*, W. H. Freeman and Co., San Francisco.

(40) Li, Y., He, W., Dong, Y., Shenga, F., and Hu, Z. (2006) Human serum albumin interaction with formononetin studied using fluorescence anisotropy, FT-IR spectroscopy, and molecular modeling methods. *Bioorg. Med. Chem. 14*, 1431–1436.

(41) Gillis, A. M., Yee, Y. G., and Kates, R. E. (1985) Binding of antiarrhythmic drugs to purified human α1-acid glycoprotein. *Biochem. Pharmacol. 34*, 4279–4282.

(42) Greenfield, N. J. (2006) Using circular dichroism spectra to estimate protein secondary structure. *Nat. Protoc. 1*, 2876–2890.

(43) Kelly, S. M., and Price, N. C. (1997) The application of circular dichroism to studies of protein folding and unfolding. *Biochim. Biophys. Acta 1338*, 161–185.

(44) Andrade, M. A., Chaco′n, P., Merelo, J. J., and Mora′n, F. (1993) Evaluation of secondary structure of proteins from UV circular dichroism spectra using an unsupervised learning neural network. *Protein Eng. 6*, 383–390.

(45) Böhm, G., Muhr, R., and Jaenicke, R. (1992) Quantitative analysis of protein far UV circular dichroism spectra by neural networks. *Protein Eng. 5*, 191–195.

(46) Greenfield, N. J. (2006) Using circular dichroism collected as a function of temperature to determine the thermodynamics of protein unfolding and binding interactions. *Nat. Protoc. 6*, 2527–2535.

(47) Shakhnovich, E. A., Hung, D. T., Pierson, E., Lee, K., and Mekalanos, J. J. (2007) Virstatin inhibits dimerization of the transcriptional activator ToxT. *Proc. Natl. Acad. Sci. U.S.A. 104*, 2372–2377.

(48) Pore, R. S. (1978) Microbial toxins, their functional role and phylogenetic validity. *BioSystems 10*, 189–198.

(49) Yudina, T. G., Konikhova, A. V., Revina, L. P., Kostina, L. I., Zalurim, I. A., and Chestukhina, G. G. (2003) Antibacterial activity of Cry- and Cyt- proteins from *Bacillus thuringiensis* ssp *israelensis*. *Can. J. Microbiol. 49*, 37–44.

(50) Park, J. H., and Saier, M. H., Jr. (1996) Phylogenetic, structural and functional characteristics of the Na-K-Cl cotransporter family. *J. Membr. Biol. 149*, 161–168.

(51) Keqian, Y. J. (2001) Prokaryotic calmodulins: Recent developments and evolutionary implications. *Mol. Microbiol. Biotechnol. 3*, 457–459.

(52) Michiels, J., Xi, C., Verhaert, J., and Vanderleyden, J. (2002) The functions of Ca^{2+} in bacteria: A role for EF-hand proteins. *Trends Microbiol. 10*, 87–93.

(53) Rigden, D. J., Jedrzejas, M. J., Moroz, O. V., and Galperin, M. Y. (2003) Structural diversity of calcium-binding proteins in bacteria: Single-handed EF-hands? *Trends Microbiol. 11*, 295–297.

(54) Tsujibo, H., and Rosen, B. P. (1983) Energetics of calcium efflux from cells of *Escherichia coli*. *J. Bacteriol. 154*, 854–858.

(55) Ambudkar, S. B., Lynn, A. R., Maloney, P. C., and Rosen, B. P. (1986) Reconstitution of ATP-dependent calcium transport from *Strptococci*. *J. Biol. Chem. 261*, 15596–15600.

(56) Trucksis, M. Accessory cholera enterotoxin and analogs thereof as activators of calcium dependent chloride channel. U.S. Patent 7,582,424 B2, September 1, 2009.

(57) Miller, S., Janin, J., Lesk, A. M., and Chothia, C. (1987) Interior and surface of monomeric proteins. *J. Mol. Biol. 196*, 641–656.